Sensors & Actuators: A. Physical 337 (2022) 113426

Contents lists available at ScienceDirect

Sensors and Actuators: A. Physical

journal homepage: www.journals.elsevier.com/sensors-and-actuators-a-physical

Validation of an automated system for the experimentation of photothermal therapies on cell cultures

José Manuel Terrés-Haro [a,*], Andy Hernández-Montoto [a,b,c,d], María Pardo-Huguet [e], Cristina de la Torre [a,b,c,d], Javier Monreal-Trigo [a], Javier Ibañez [a], Rafael Masot-Peris [a], Ramón Martínez-Máñez [a,b,c,d], Eduardo García-Breijo [a]

[a] Instituto Interuniversitario de Investigación de Reconocimiento Molecular y Desarrollo Tecnológico (IDM), Universitat Politècnica de València, Universitat de València, Camino de Vera s/n, 46022 Valencia, Spain
[b] CIBER de Bioingeniería, Biomateriales y Nanomedicina (CIBER-BBN), Spain
[c] Unidad Mixta UPV-CIPF de Investigación en Mecanismos de Enfermedades y Nanomedicina, Universitat Politècnica de València, Centro de Investigación Príncipe Felipe, Valencia, Spain
[d] Unidad Mixta de Investigación en Nanomedicina y Sensores. Universitat Politècnica de València, IIS La Fe, Valencia, Spain
[e] Universitat Politècnica de València, Camino de Vera s/n, 46022 Valencia, Spain

ARTICLE INFO

Keywords:
Hyperthermia
Electronic devices
Lab automation
Therapy planning

ABSTRACT

Hyperthermia is a technique used in treatments against cancer, consisting in heating the cancerous tissue to 40–44 ˚C to produce apoptosis. The addition of noble metal nanoparticles would suppose a great progress in this technique development, due to their ability to produce heat or release drugs in or near the cancer cells when irradiated at a certain wavelength.

This paper presents the validation of a prototype automated system for the basic experimentation of hyperthermia mediated by nanoparticles on cell cultures. It consists of a laser beam irradiating the samples placed in a 2D moving mechanism, an ambient temperature control to keep the samples in an incubation temperature range, and a thermographic camera to measure the temperature achieved. The system is controlled from a computer by a graphical user interface. The validation is done first in a suspension of gold nanostars and water to validate the temperature ranges, and then in SK-Mel and HeLa cell cultures, with varying concentrations and exposure times and measuring the cell viability 24 h after. These experiments showed that the treatment is possible and will cause cell death within a certain range of the variables to be applied. Also, an in-silico model of gold nanoparticle and its suspension in water was developed to try to predict the temperatures achieved during the treatment. The results of this model simulations are compared with the experiment results.

1. Introduction

For the last 5 millennia hyperthermia has been an ever-developing technique for the treatment of tumors. It is said that the ancient Greek Hippocrates foresaw the use of heat for this purpose [1]. The rationale of this treatment is based in the influence of temperature over the cell survivability in an already malfunctioning tissue that may have poor blood and oxygen supply, creating an environment of low pH and hypoxic cells that may not be able to survive the shock of an increase in temperature to a range of 40–44 ˚C, while leaving the healthy tissue undamaged [2]. More recently, the application of heat has been found to activate cellular pathways that cause a sensitization of the malignant tissue to chemo and radiotherapy, which lead to the use of hyperthermia alongside these conventional treatments, proving that the synergy between them provides better results in a combined therapy that one of them individually [3–5].

The development of nanotechnology brought the use of metallic nanoparticles to hyperthermia, due to their physical and biological characteristics [6]. Noble metal nanoparticles show an excitation of the electron cloud localized in their surface when irradiated at a certain wavelength, called the surface plasmon resonance (SPR) wavelength, which is then dampened through radiation or relaxation mediated by electron-phonon collisions, producing heat [7]. In optical terms, this causes the nanoparticles to have an absorption cross-section much larger

* Corresponding author.
E-mail address: jmterres@upv.es (J.M. Terrés-Haro).

https://doi.org/10.1016/j.sna.2022.113426
Received 2 September 2021; Received in revised form 11 January 2022; Accepted 3 February 2022
Available online 9 February 2022

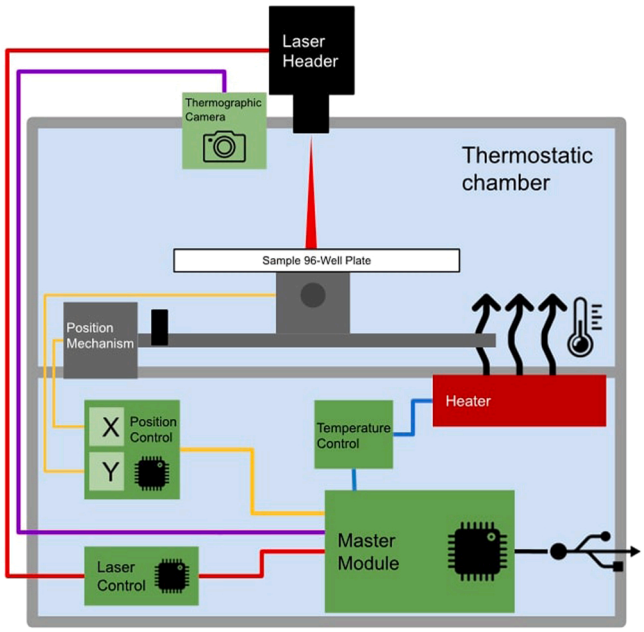

Fig. 1. Representation of the distribution and block diagram of the components integrated into the hyperthermia equipment.

than its geometrical cross-section, which results in a very efficient conversion of light into heat [8]. The SPR wavelength location is determined by the material and the geometry of the nanoparticle, so it can be tuned to the most convenient parameters, which resulted in a wide variety of possibilities [9]. The most used material for this application is gold due to its biocompatibility, proving to be non-toxic, and its geometry is tuned so the SPR wavelength is in the near-infrared range, so the excitation light is capable to penetrate deeper into the tissue [10,11]. The particle excitation is intended to be used to produce heat and release drugs near, or inside, the tumor cells, providing a localized treatment that combines the advantages of both hyperthermia and a contained chemotherapy, which should reduce the secondary effects compared to a chemotherapy that spreads to the whole body [12,13]. The use of light to treat medical conditions, along with the addition of photosensitizers such as dyes to increase its efficiency, also dates from thousands of years ago, which is the field of photothermal therapies (PTT) [14,15]. It is now with the development of all the fields surrounding it that we can exploit its full potential.

One challenge this proposed treatment is facing is the differentiation between hyperthermia and ablation. Hyperthermia should contribute to apoptosis, while ablation, a few degrees above, is causing necrosis. Ablation might be unsortable as the temperature in the vicinity of the nanoparticles increases very fast, reaching hundreds of degrees [16], and it is known that cells that absorbed the nanoparticles might collapse in thousands of a second due to cavitation [17], but its effects may be limited if a good selection of nanoparticle concentration and control of irradiation is applied.

Due to the surging nature of this research, there is a demand for technology to test the new approaches, which requires multiple iterations and the replication of experiments to ensure the viability of the designed treatment. The main proposal is the design of an electronic system, including hardware and user interface, to ease the experimentation on the toxicity of the nanoparticles in cell cultures and the effects provided when irradiated with a laser, such as a review of heat generation efficiency and cell survival. In addition, in-silico models of a nanoparticle and of a suspension of nanoparticles have been developed to try to predict the thermal effects of the laser irradiation.

The design is based on the previous work of the group, featuring an 808 nm laser and a thermostatic chamber [18], where the samples to be irradiated were placed manually under the beam, showing numerous drawbacks due to its proof-of-concept character. The new design is to have multiple samples placed automatically under the laser beam by a 2D platform, avoiding contact with the sample plate between experiments, and the circuitry design is completely renewed to make it more robust.

The system is tested in two ways: first using a solution of gold nanoparticles in distilled water and measuring the temperature rise, and secondly in cell cultures of HeLa and SK-MEL cell lines, measuring temperature and cell viability at different time and nanoparticle concentration. The same variables of the system validation experiments are used for the computation of the in-silico models, and the results will be compared.

2. Methodology

The methodology is divided between the description of the designed system, including hardware and software, the development of in-silico models, and the description of the experiments that took place for the validation of the system.

2.1. Hardware

The hardware solution proposed to automatize the hyperthermia experimental procedures was the hyperthermia equipment, schematized in the Fig. 1 and summarized in the following points.

2.1.1. Electronics and Control

The electronics are divided in 5 modules:

The **Main Module**, with a 32-bit Atmel SAM3X8E microcontroller, its main tasks are to communicate with the graphical user interface (GUI), receive commands and pass them to the rest of the modules to perform the experiments, control the system in real time, and monitor the sensors.

A **Positioning Control Module**, which actuates on two stepper motors on a sample positioning mechanism to place the samples under the laser beam. It uses two limit switch sensors as initial points to start the count of steps needed to reach each sample (zero point), and then moves between the samples in an open loop control using two A4988 stepper drivers. The position of each well in the 96-Well plate is precalibrated and saved into its ATMega328P microcontroller.

The laser beam power is proportional to the current passing by the laser diode. The **Laser Control Module** is a voltage to current converter with a 12-bit digital to analog converter (DAC) used as reference. A relay is placed right before the laser diode to prevent damage due to current transients during activation or wearing due to parasitic currents. This module uses an ATTiny85 to control the relay and monitor the current through the laser diode.

The temperature in the thermostatic chamber where the samples are placed is controlled by reading a DS18B20 sensor connected to the Main Module. The Main Module sets an input in the **Ambient Temperature Control Module** to command the activation of a 100 W ceramic heater and a fan to introduce hot air into the chamber until the ambient temperature reaches the reference. This module is separated from the Main Module for a better management of the high current surges and power dissipation needed, also it has an analog protection circuitry to stop the heater if the fan does not work, avoiding overheating. Finally, an AMG8833 8 $\times$ 8 pixel **Thermographic Camera Module** is placed by the laser header and pointing to the sample that is being irradiated to measure its temperature evolution.

2.1.2. Mechanism

The placement of the samples below the laser beam is done using a 2-D mechanism with two stepper motors and one limit switch sensor on the zero point of each axis. The samples, in a 96-Well plate, are placed in the upper table.

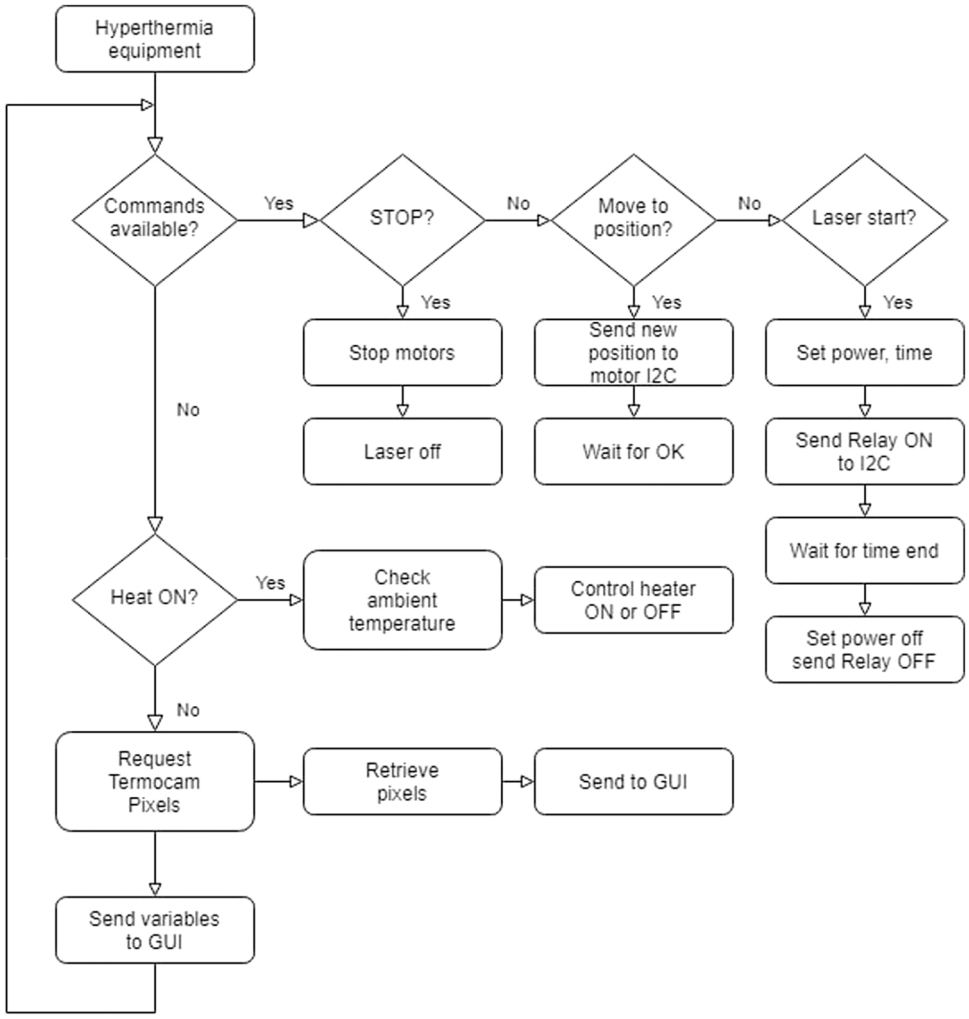

Fig. 2. Flow diagram of the firmware.

2.1.3. Laser header

The 808 nm and 500 mW laser diode is contained in a heatsink structure and an adjustable collimator lens is placed in front of it to achieve the desired irradiance spot at the sample. The collimator distance to the laser diode is calibrated so the spot irradiance on the surface of the samples table is 4 W cm^{-2} at 500 mW output power [18].

2.1.4. Structure

The system is supported by a structure of transparent methacrylate in a box shape, with two stacked chambers, from top to bottom: one thermostatic chamber in which the positioning mechanism, the laser header and the samples to be processed are placed; and another with the electronics needed to measure, control and actuate on the aforementioned features.

2.2. Firmware

The firmware that is burned into the hyperthermia equipment can be summarized as seen in Fig. 2.

2.3. Software

Two separated user interfaces were developed using Processing [19]:

2.3.1. Experiment planification interface

This interface is a planification program where the samples to be irradiated into a 96-Well plate can be selected, each one with different parameters (time, laser power), and irradiation order. The planning is saved into a file to be read later by the hyperthermia control interface.

2.3.2. Hyperthermia control interface

This interface is used to read the planification file and communicate via USB with the system hardware, it sends the necessary commands to perform the planned experiments, and receives sensor information from the hardware, displaying it to the user in a way which is easier and faster to understand. A summary of its functions can be seen in the flow diagram of Fig. 3.

2.4. In-Silico models

Two in-silico models were prepared using Comsol Multiphysics 5.5 to try to predict the results during the experimentation. The description of the models will be brief as it is not the scope of this paper.

2.4.1. Gold nanoparticle interaction with NIR laser

The individual gold nanoparticle model is done with the ideal and parametric geometry of a gold nanostar, and its electromagnetic interaction with a coherent light is studied [16,20]. The parameters are tuned so the absorption spectrum of the individual nanoparticle has its peak near the 808 nm wavelength, that of the laser to be used, resembling the nanoparticles and measurements from the synthesis that is used later on the experiments. The observed result for the further development of a

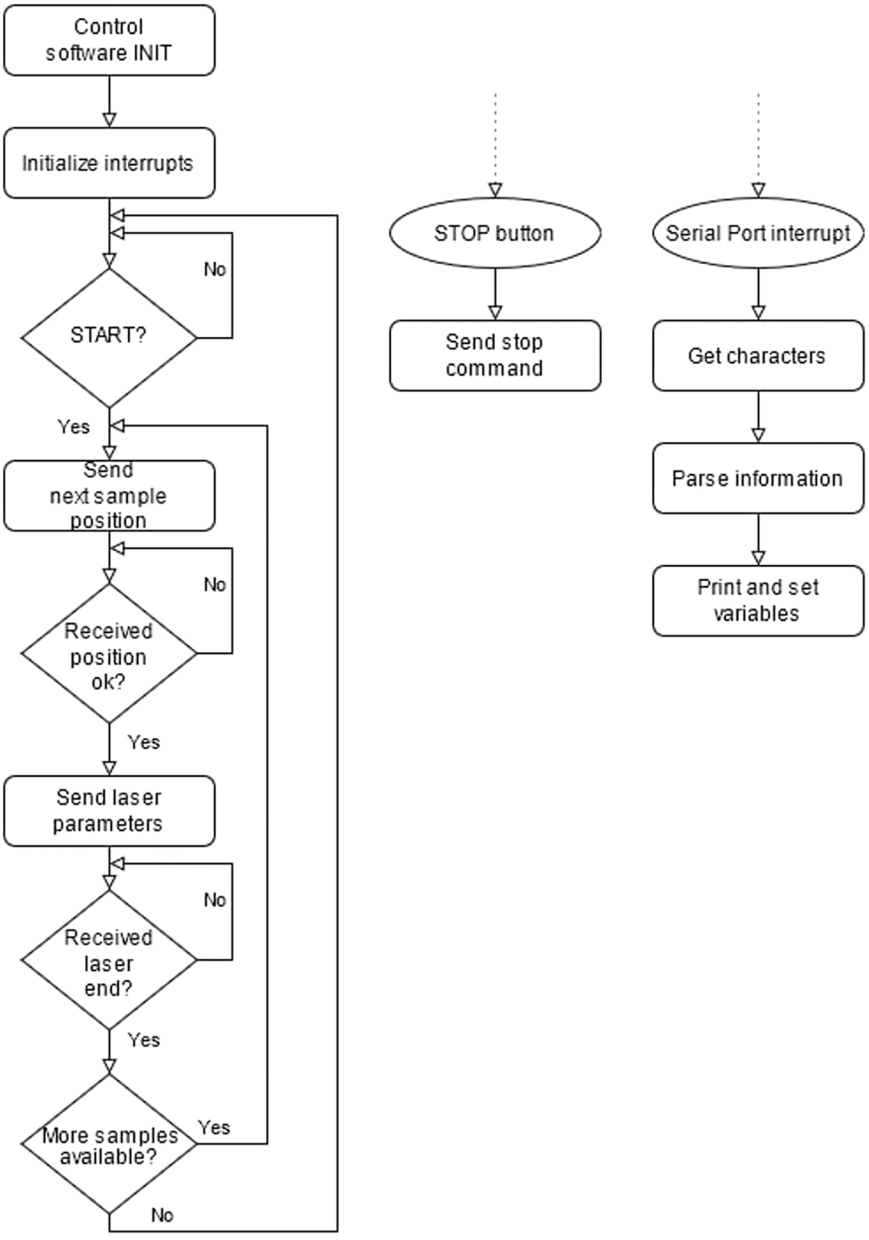

Fig. 3. Flow diagram of the Hyperthermia control interface software.

prediction model is the approximate heat generation of each nanoparticle under a given laser beam power.

2.4.2. 96-Well experiment simulation

This model pretends to predict the temperature rise during the irradiation of a nanoparticles and distilled water solution placed in a 96-Well plate well.

In a simplified model, the heat generation of each nanoparticle is multiplied by the number of nanoparticles under a laser beam in a solution sample being irradiated, giving as a result a given heat by the irradiated volume [21,22]. Heat dissipation effects are added in the boundaries. The main result extracted from this model was the temperature given by a function of laser power, nanoparticle concentration and irradiation time.

2.5. Validation experiment

For this validation experiment a 5.4 mmol suspension of gold nanostars in distilled water was used. First, two experiments were done using 200 μL of the stock suspension, irradiating them both with 4 W cm^{-2} for 5 min and measuring the temperature curves with the integrated thermographic camera and a Photon Control FTC-DIN-GT-ST-LNY2 fiber optic temperature probe. The results were used to adjust the in-silico model.

Next, four 200μL suspensions of 5.4 mmol were irradiated with 4, 2, 1 and 0.5 W cm^{-2} for 5 min each, measuring the temperatures only with the thermographic camera, obtaining different maximum temperatures. Finally, two 200 µL suspensions of 2.7 and 1.35 mmol were irradiated with 2 W cm^{-2} for 5 min each, measuring temperature.

2.6. Cell viability assays

2.6.1. Cell growing

HeLa cells were grown at 37 ˚C under humidified air containing CO_2 (5 vol%) in Dulbecco's modified Eagle's medium (DMEM), which was supplemented with fetal bovine serum (10 vol% FBS) and penicillin/

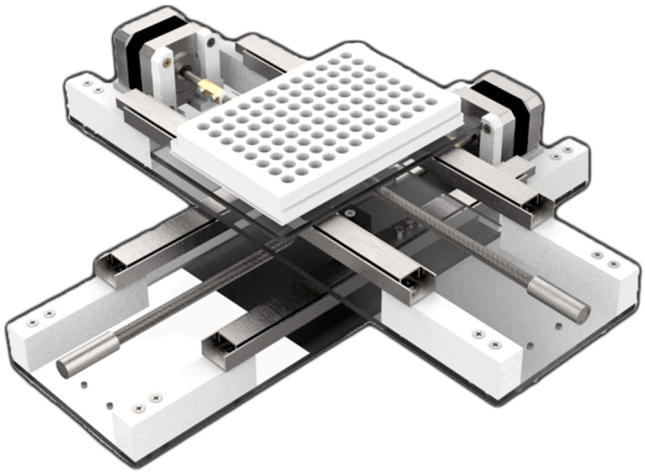

Fig. 4. Render of the design of the 2D sample placing mechanism used in the hyperthermia equipment.

streptomycin (1 vol%; 10,000 units of both per mL). After 24 h of incubation, cells were rinsed with phosphate-buffered saline (PBS), and then detached with trypsin (0.2 vol%)/PBS. The HeLa cells were seeded in 96-well plates (density of 2×10^3 cells per well) and grown in DMEM for 24 h.

This procedure was identical for SK-MEL cells, except it took more incubation time to achieve the same cell density.

2.6.2. Gold nanostar preparation

Bare gold nanostars obtained by the seeded growth method [23] were sterilized in UV light for 20 min. A dilution of nanoparticles was prepared using half volume of stock gold nanostars and half distilled water, achieving a concentration of 2.7 mmol. Parting from 1 µL of this dilution, the gold nanoparticles were washed twice with distilled water by centrifugation (20 min 9500 rpm) and redispersion.

2.6.3. Cytotoxicity assays

HeLa and SK-MEL cells were used to find which is the range of nanoparticle concentration in the growth medium that will not be toxic without applying the hyperthermia treatment.

For this, the cells in DMEM were treated with nanoparticles suspension to achieve concentrations between 25 and 200 µg mL^{-1} with an exposure time of half an hour, then the cells were washed with PBS and clean DMEM and left to grow for another 24 h in the aforementioned growing conditions. This was done with 16 samples for each nanoparticle concentration and other 16 samples were added as control without nanoparticles.

The cytotoxicity measurements were done 24 h after the exposure of the cells to the treatment, by the colorimetric assay of cellular metabollic activity using MTT (3-(4,5-dimethylthiazol-2-yl)− 2,5-diphenyltetrazolium bromide) tetrazolium reduction [24].

2.6.4. Laser exposure assays

The hyperthermia assays on HeLa cells were done by triplicated, varying the nanoparticle concentration that was applied and the irradiation time, keeping constant the irradiation power (4 W cm^{-2}). An irradiation control without nanoparticles was performed to confirm that the laser exposure has no effects over cell viability [25].

The cells were treated with nanoparticles suspension and DMEM in concentrations between 10 and 100 µg mL^{-1} and were irradiated during 5, 10 and 15 min. Once the experiments were done, the cell medium was washed with PBS and DMEM and left in growing conditions. The cell viability was measured 24 h after the treatment with the MTT assay.

The SK-MEL assays were done following the same steps but only once due to the lack of stock nanoparticles from the same synthesis.

Fig. 5. Laser support and thermographic camera.

Fig. 6. Render of the design of the structure that contains the hardware.

3. Results

The results are divided in the same way as the methodology.

3.1. Hyperthermia system

The hyperthermia system is separated into hardware and user interfaces.

3.1.1. Hardware

Herein we present the resulting structures and mechanisms as renders of their CAD design for better clarity. First, the sample placing mechanism in Fig. 4 where both axes of movement and the placement of the 96-well plate can be seen. Next, in Fig. 5 is represented the heatsink where the laser diode is placed, on top of a support to achieve the desired distance to the sample and therefore the calibrated irradiance. The cable emerging from the center is a USB camera for the calibration of the

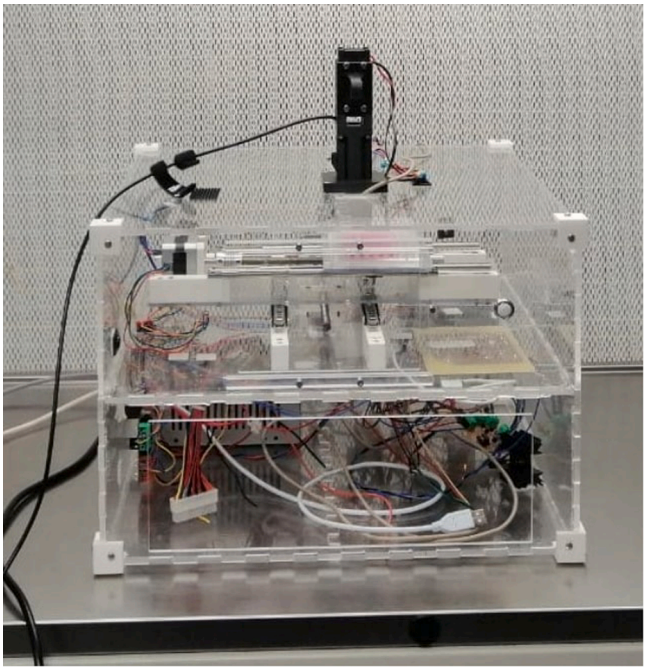

Fig. 7. Hyperthermia equipment prototype.

positioning mechanism, and on its right is the AMG8833 thermographical camera with its own support at an angle to aim directly on the surface of the sample. Finally, in Fig. 6 there is a render of the external structure, a box of methacrylate, that contains the hardware.

For the illustration of the resulting assembly, the real prototype can be seen in Fig. 7.

3.1.2. User Interfaces

The planification interface in Fig. 8 consists on a matrix of circles like the ones in the 96-well plate. When clicking over one of the circles, the variables in the right side boxes are saved for that well. The data can be seen by hovering over the circle. Different colors are available for planification, and a priority number can be assigned to change the order of irradiation.

The control interface in Fig. 9 connects to the hyperthermia equipment with the serial communication menu in the upper left corner, the buttons next to it are used to load the previously planned experiment, and start or skip the irradiation of samples. The sample that is being irradiated is shown in red, and its variables displayed. Two buttons control the 2D sample placing mechanism when it is not performing an experiment, one to place the samples near the entrance of the box, and another to move the mechanism to its zero point. In the right side there is one stop button to abort the active command, and the variables sent by the equipment are displayed, including ambient temperature, laser power and the image from the thermographic camera, after the double application of a bilinear interpolation.

3.2. In-silico models

The nanoparticle model parameters were adjusted resembling the core and spike sizes of previously synthesized samples, and then finely tuned to have its Surface plasmon resonance wavelength at approximately 808 nm, resulting in the Fig. 10 geometry.

Each iteration a wavelength sweep was performed to check the situation of the peak absorption cross-section, finally resulting in a spectrum as seen in Fig. 11.

The nanoparticle solution in a well model which geometry is represented in Fig. 12 reported results close to the measured temperatures during the experiments with the most notable difference being the derivative of the curve. As there were most probably differences between the real environment and the simulation, as air conditioning or natural air gusts, the dissipation parameters were adjusted so the simulation result would match a calibration heating curve measured during the experiments, resulting in the Fig. 13 curves.

3.3. Nanostars heating in water

The Fig. 14 shows the results of the experiments of the dissolution of nanoparticles in water and the comparison with their analog in the simulation for the case of equal concentrations and different irradiation power.

Fig. 15 shows the results of the experiments and the comparison with the simulation in the case of different concentrations and equal irradiation power. Decreasing temperatures can be seen in the first seconds because the thermographical camera is logging the hottest spot, therefore sampling the temperature from the last adjacent sample irradiation.

These results, both simulated and experimental, show that there

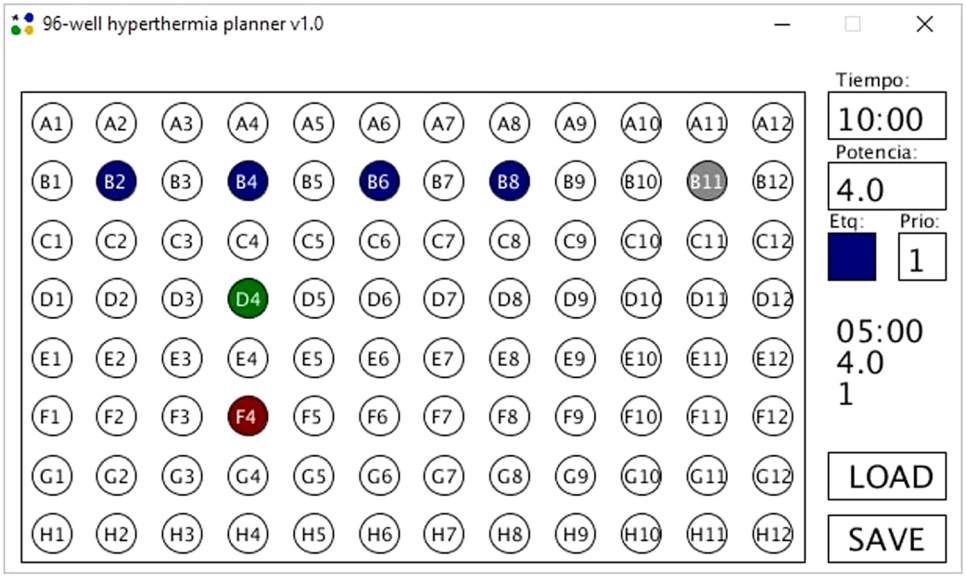

Fig. 8. Hyperthermia experiment planner GUI.

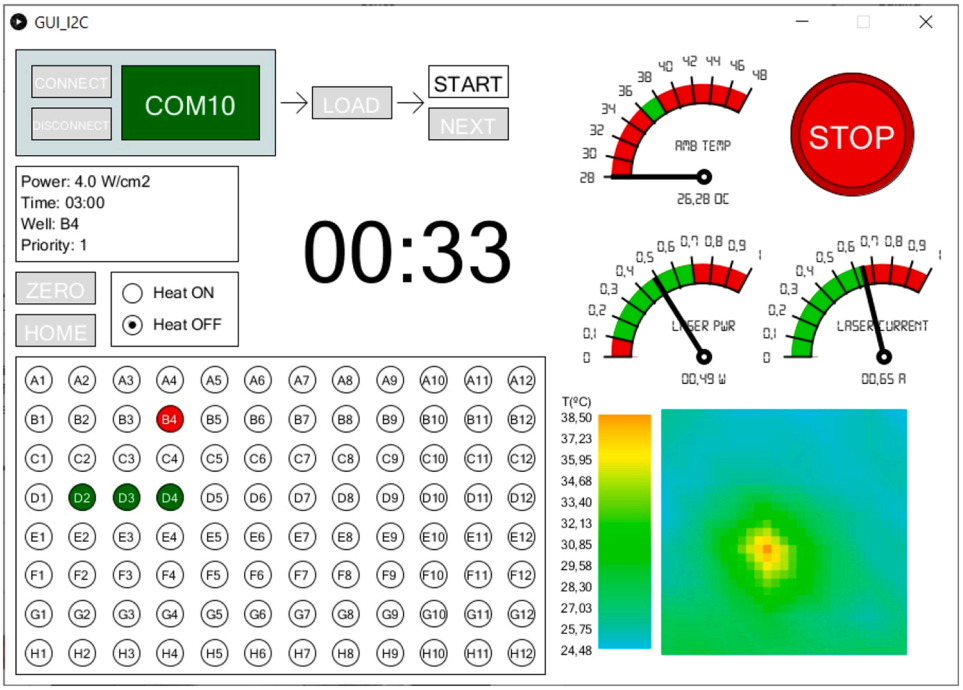

Fig. 9. Hyperthermia system control interface.

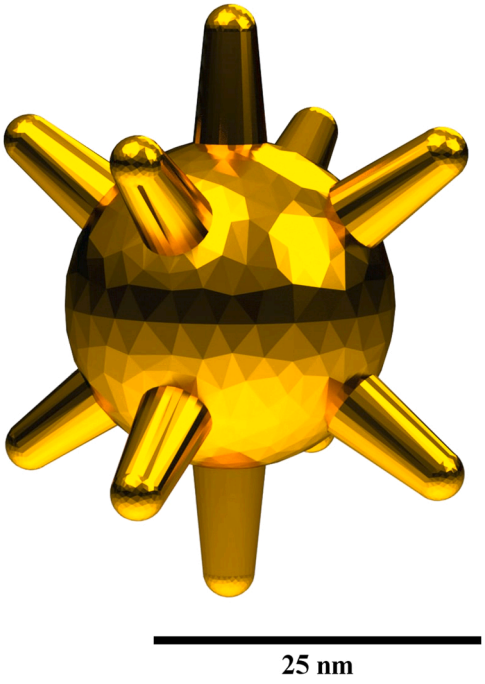

Fig. 10. Nanostar geometry used in the modelization.

exists a range of intermediate concentrations in which the temperature rise is higher. It is reasonable that this effect is due to the high absorption coefficient obtained from the application of the Beer-Lambert law on higher concentrations, resulting in the absorption of the laser in the first micrometers of the sample, where heat is easily dissipated to air. Nonetheless, the overall resulting conclusion from these experiments is that hyperthermia temperature range is achievable with the use of the developed equipment.

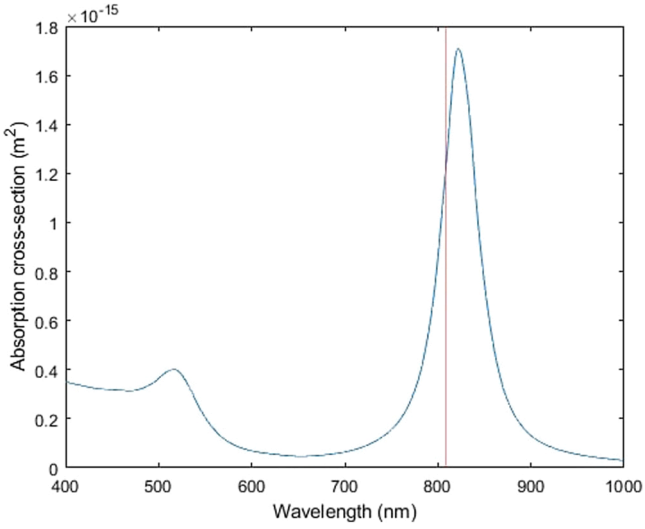

Fig. 11. Individual gold nanostar-like model absorption cross-section in the spectrum, adjusted to peak near the central emission wavelength of an 808 nm laser (marked in red).

3.4. Cell viability assays

Finally, the results for cell viability in HeLa and SK-MEL cultures are presented.

3.4.1. HeLa

First, the control citotoxicity for nanoparticle concentration without laser irradiation in HeLa cells can be seen in Fig. 16. Results show that the concentrations between 25 and 75 μg mL^{-1} result in null toxicity, but will produce a limited toxicity at 100 μg mL^{-1}. Higher concentrations have been found unsuitable for this application as they produce severe toxicity.

When irradiated at non-toxic concentrations and different times, the

Fig. 12. Well model geometry.

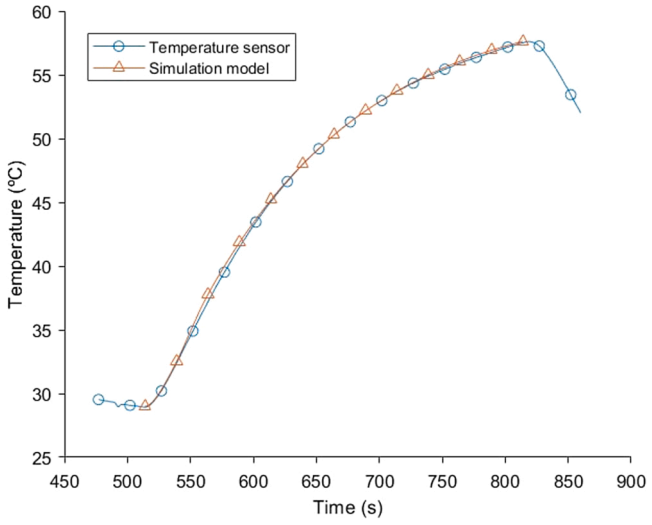

Fig. 13. Experimental measured curve compared with the one obtained with the adjusted model.

results show that cell death is not relevant for concentrations between 10 and 25 μg mL^{-1}, and will start to be perceived at 50 μg mL^{-1}. With 100 μg mL^{-1} cell death is considered very high. These results are summarized in Fig. 17.

3.4.2. SK-MEL

For SK-MEL cells, the results are similar. Complete viability of the samples is found at 25 μg mL^{-1}, and a reduced toxicity up to

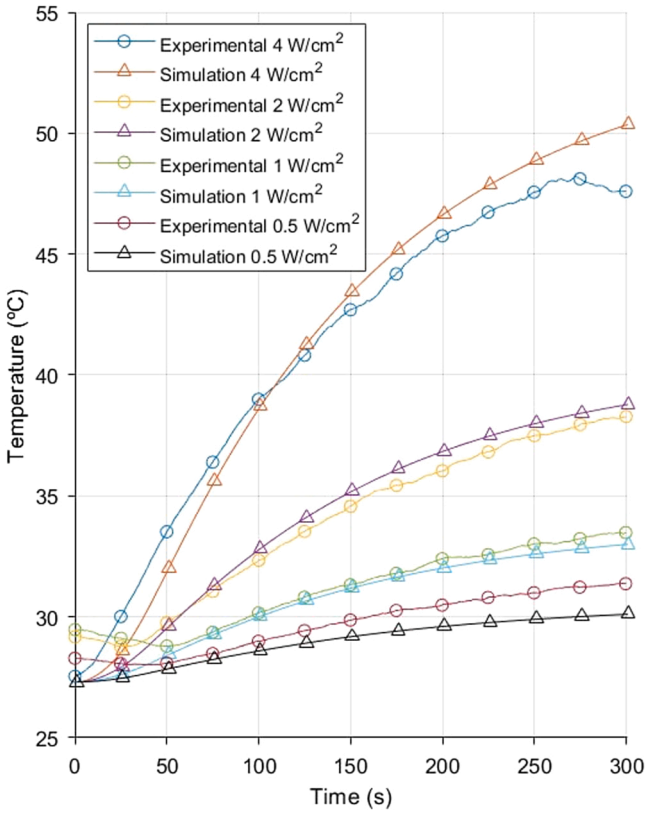

Fig. 14. Temperature evolution in experimental and simulation irradiation of 5.4 mmol samples at different irradiation power, ranging from 0.5 to 4 W cm^{-2}.

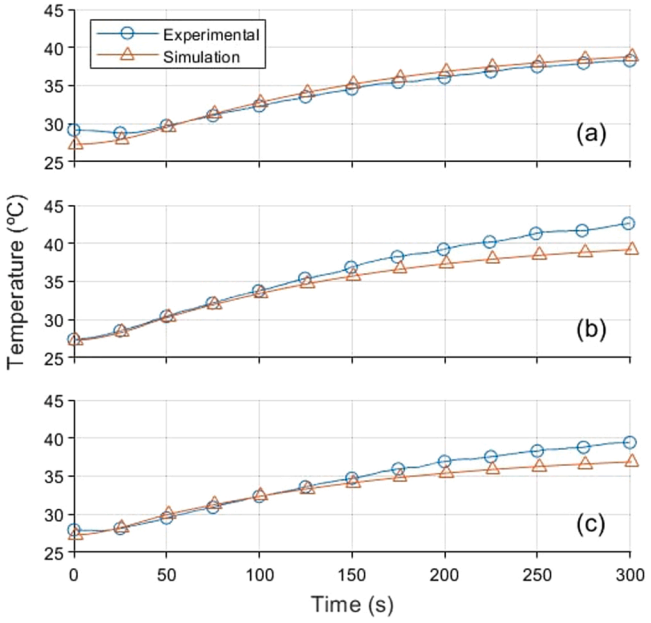

Fig. 15. Temperature evolution in experimental and simulation irradiation of different concentration samples (a) 5.4 mmol (b) 2.7 mmol (c) 1.35 mmol at 2 W cm^{-2}.

100 μg mL^{-1}, with an excessive toxicity for this application in the case of 150 μg mL^{-1}, as can be seen in Fig. 18.

In this case the effects of the treatment seem to be much more pronounced, only certain mortality can be observed at 25 μg mL^{-1}. With 50 μg mL^{-1}, mortality is high, and almost total mortality can be

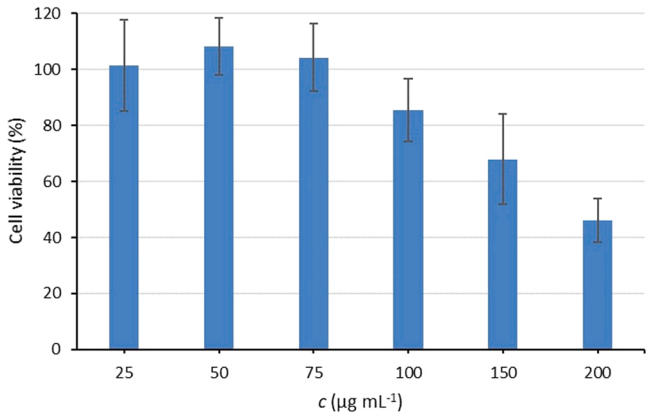

Fig. 16. HeLa citotoxicity.

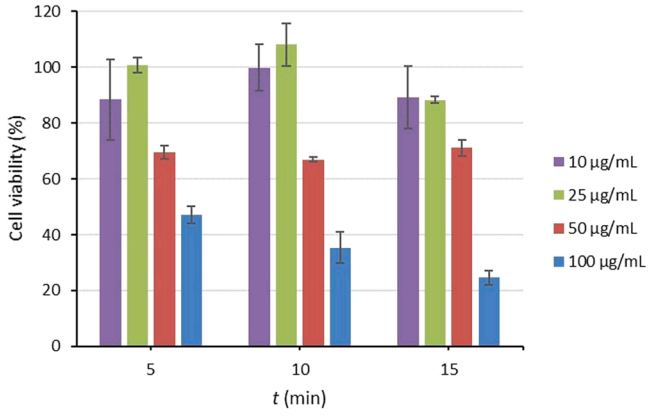

Fig. 17. HeLa hyperthermia treatment viability.

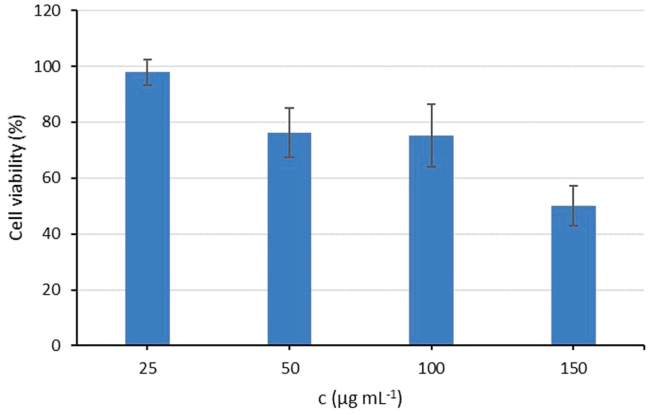

Fig. 18. SK-MEL citotoxicity.

considered when 100 µg mL^{-1} are applied. The data obtained is represented in Fig. 19.

4. Conclusions

The resulting system is a programmable device for hyperthermia experimentation with capability for the use of different laser powers, irradiation times, automatic positioning of samples in a 96-Well plate and ambient temperature control. This system has been tested in conditions similar to those expected under real use, in cell viability experiments, and yielded results as expected. The system eased the process of

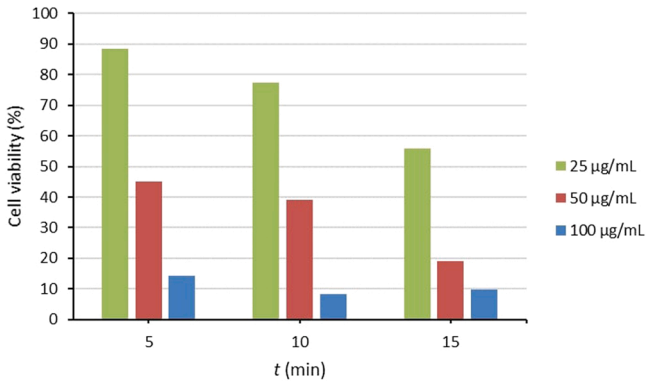

Fig. 19. SK-MEL hyperthermia treatment viability.

experimentation, reducing the manipulation time required to carry out multiple irradiations, when compared with the manual method used before its conception. Also, the developed prototype is capable of monitoring and logging the sample temperature in real time, which allowed us to collect and process data about the sample response to irradiation, and will allow to apply a control on the laser power to avoid exceeding the expected temperature range for the treatment.

The prototype was first tested with suspensions of gold nanostars in distilled water, where the general functioning of the system and its ability to perform further in-vitro experiments was verified, obtaining the temperature curves shown in the results. Then the in-vitro viability experiments were carried out on HeLa and SK-Mel cells, yielding results that indicate that the treatment is able to kill the cancerous cells when irradiating samples treated with a 50–100 µg mL^{-1} suspension of nanoparticles.

Although it was specified that the use of the equipment would be for in-vitro experimentation, some features were added in anticipation to further development of the photothermal treatment, increasing its adaptability to future ex-vivo or in-vivo experiments, for example with tissue samples or small enough animals. The additions include the software to use the calibration camera to target the sample region of interest with the laser. Furthermore, another system is being developed with a different targeting philosophy to meet the expectations transmitted from a laboratory that works with animals.

The in-silico models provide fundamental data for the understanding and future development of nanoparticles with different materials and geometries to efficiently exploit their plasmonic properties. They are also a good start for the development of more complex environments to finally predict the outcomes of a treatment. In this study, we developed a model to calculate the temperature curve that should result from the in vitro experiments, and validated it by comparing the data from the model with the data from the experiments, which resulted to be similar. Some changes are needed in the actual model, as applying the loss of plasmonic properties due to melting of the nanoparticles, which results in a plateau in the temperature evolution at larger times.

CRediT authorship contribution statement

José Manuel Terrés-Haro: Conceptualization of this study, Methodology, Software, Investigation, Formal analysis, Data curation, Writing draft, Visualization. **Andy Hernández**: Conceptualization of this study, Methodology, Resources. **María Pardo-Huguet**: Methodology, Software, Validation, Investigation, Formal analysis. **Cristina de la Torre**: Conceptualization of this study, Methodology, Validation, Supervision, Resources. **Javier Monreal-Trigo**: Software, Formal analysis, Writing review. **Javier Ibañez**: Conceptualization of this study, Supervision, Writing – review and editing. **Rafael Masot-Peris**: Conceptualization of this study, Supervision, Writing – review and editing. **Ramón Martínez-Máñez**: Conceptualization of this study, Supervision,

Resources, Funding acquisition. **Eduardo García-Breijo**: Supervision, Resources, Funding acquisition, Project administration.

Declaration of Competing Interest

The authors declare that they have no known competing financial interests or personal relationships that could have appeared to influence the work reported in this paper.

Acknowledgments

We thank the financial support from the Spanish Government (projects RTI2018-100910-B-C41, RTI2018-100910-B-C43 and FPU17/03800) and the Generalitat Valenciana (project PROMETEO 2018/024). Funding for open access charge: CRUE-Universitat Politècnica de València.

References

[1] E.S. Glazer, S.A. Curley, The ongoing history of thermal therapy for cancer, Surg. Oncol. Clin. North Am. 20 (2) (2011) 229–235, https://doi.org/10.1016/j.soc.2010.11.001.
[2] J. van der Zee, Heating the patient: a promising approach? Ann. Oncol. 13 (8) (2002) 1173–1184, https://doi.org/10.1093/annonc/mdf280.
[3] P. Wust, B. Hildebrandt, G. Sreenivasa, B. Rau, J. Gellermann, H. Riess, R. Felix, P. Schlag, Hyperthermia in combined treatment of cancer, Lancet Oncol. 3 (8) (2002) 487–497, https://doi.org/10.1016/S1470-2045(02)00818-5.
[4] P. Kaur, M.D. Hurwitz, S. Krishnan, A. Asea, Combined hyperthermia and radiotherapy for the treatment of cancer, Cancers 3 (4) (2011) 3799–3823, https://doi.org/10.3390/cancers3043799.
[5] A. Oei, H. Kok, S. Oei, M. Horsman, L. Stalpers, N. Franken, J. Crezee, Molecular and biological rationale of hyperthermia as radio- and chemosensitizer, Adv. Drug Deliv. Rev. 163–164 (2020) 84–97, https://doi.org/10.1016/j.addr.2020.01.003.
[6] K. McNamara, S.A. Tofail, Nanoparticles in biomedical applications, Adv. Phys. X 2 (1) (2017) 54–88, https://doi.org/10.1080/23746149.2016.1254570.
[7] M. Kim, J.H. Lee, J.M. Nam, Plasmonic photothermal nanoparticles for biomedical applications, Adv. Sci. 6 (17) (2019), https://doi.org/10.1002/advs.201900471.
[8] R. Rodríguez-Oliveros, J.A. Sánchez-Gil, Gold nanostars as thermoplasmonic nanoparticles for optical heating, Opt. Express 20 (1) (2012) 621–626, https://doi.org/10.1364/oe.20.000621.
[9] S. Govindaraju, K. Yun, Synthesis of gold nanomaterials and their cancer-related biomedical applications: an update, 3 Biotech 8 (2) (2018), https://doi.org/10.1007/s13205-018-1137-y.
[10] A. Hernández Montoto, R. Montes, A. Samadi, M. Gorbe, J.M. Terrés, R. Cao-Milán, E. Aznar, J. Ibañez, R. Masot, M.D. Marcos, M. Orzáez, F. Sancenón, L. B. Oddershede, R. Martínez-Máñez, Gold nanostars coated with mesoporous silica are effective and nontoxic photothermal agents capable of gate keeping and laser-induced drug release, ACS Appl. Mater. Interfaces 10 (33) (2018) 27644–27656, https://doi.org/10.1021/acsami.8b08395.
[11] C. Ash, M. Dubec, K. Donne, T. Bashford, Effect of wavelength and beam width on penetration in light-tissue interaction using computational methods, Lasers Med. Sci. 32 (2017) 1909–1918, https://doi.org/10.1007/s10103-017-2317-4.
[12] D. Jaque, L. MartínezMaestro, B. del Rosal, P. Haro-Gonzalez, A. Benayas, J. L. Plaza, E. Martín Rodríguez, J. García Solé, Nanoparticles for photothermal therapies. Nanoscale 6 (16) (2014) 9494–9530, https://doi.org/10.1039/c4nr00708e.
[13] A. Hernández-Montoto, M. Gorbe, A. Llopis-Lorente, J.M. Terrés, R. Montes, R. Cao-Milán, B. Díaz de Greñu, M. Alfonso, M. Orzaez, M.D. Marcos, R. Martínez-Máñez, F. Sancenón, A NIR light-triggered drug delivery system using core-shell gold nanostars-mesoporous silica nanoparticles based on multiphoton absorption photo-dissociation of 2-nitrobenzyl PEG, Chem. Commun. 55 (61) (2019) 9039–9042, https://doi.org/10.1039/c9cc04260a.
[14] A.C. Doughty, A.R. Hoover, E. Layton, C.K. Murray, E.W. Howard, W.R. Chen, Nanomaterial applications in photothermal therapy for cancer, Materials 12 (5) (2019), https://doi.org/10.3390/ma12050779.
[15] X. Li, J.F. Lovell, J. Yoon, X. Chen, Clinical development and potential of photothermal and photodynamic therapies for cancer, Nat. Rev. Clin. Oncol. 17 (11) (2020) 657–674, https://doi.org/10.1038/s41571-020-0410-2.
[16] L. Jauffred, A. Samadi, H. Klingberg, P.M. Bendix, L.B. Oddershede, Chem. Rev. 119 (13) (2019) 8087–8130, https://doi.org/10.1021/acs.chemrev.8b00738.
[17] Z. Qin, J.C. Bischof, Thermophysical and biological responses of gold nanoparticle laser heating, Chem. Soc. Rev. 41 (3) (2012) 1191–1217, https://doi.org/10.1039/c1cs15184c.
[18] R. Montes-Robles, A. Hernández, J. Ibáñez, R. Masot-Peris, C. de la Torre, R. Martínez-Máñez, E. García-Breijo, R. Fraile, Design of a low-cost equipment for optical hyperthermia, Sens. Actuators A: Phys. 255 (2017) 61–70, https://doi.org/10.1016/j.sna.2016.12.018.
[19] The Processing Foundation, Processing 3.5.4. 2019. ⟨https://processing.org/⟩.
[20] H. Yuan, C.G. Khoury, H. Hwang, C.M. Wilson, G.A. Grant, T. Vo-Dinh, Gold nanostars: surfactant-free synthesis, 3D modelling, and two-photon photoluminescence imaging, Nanotechnology 23 (7) (2012), https://doi.org/10.1088/0957-4484/23/7/075102.
[21] R. Mooney, E. Schena, P. Saccomandi, A. Zhumkhawala, K. Aboody, J.M. Berlin, Gold nanorod-mediated near-infrared laser ablation: in vivo experiments on mice and theoretical analysis at different settings, Int. J. Hyperth. 33 (2) (2017) 150–159, https://doi.org/10.1080/02656736.2016.1230682.
[22] J. Mesicek, K. Kuca, Summary of numerical analyses for therapeutic uses of laser-activated gold nanoparticles, Int. J. Hyperth. 34 (8) (2018) 1255–1264, https://doi.org/10.1080/02656736.2018.1440016.
[23] A. Hernandez Montoto, A. Llopis-Lorente, M. Gorbe, J.M. Terrés, R. Cao-Milán, B. Diaz de Greñu, M. Alfonso, J. Ibañez, M.D. Marcos, M. Orzáez, R. Villalonga, R. Martínez-Máñez, F. Sancenon, Janus gold nanostars-mesoporous silica nanoparticles for NIR light-triggered drug delivery, Chem. - A Eur. J. 25 (32) (2019) 8471–8478, https://doi.org/10.1002/chem.201900750.
[24] S. Kamiloglu, G. Sari, T. Ozdal, E. Capanoglu, Guidelines for cell viability assays, Food Front. 1 (3) (2020) 332–349, https://doi.org/10.1002/fft2.44.
[25] A. Cios, M. Cieplak, Ł. Szymański, A. Lewicka, S. Cierniak, W. Stankiewicz, M. Mendrycka, S. Lewicki, Effect of different wavelengths of laser irradiation on the skin cells, Int. J. Mol. Sci. 22 (5) (2021), https://doi.org/10.3390/ijms22052437.

José Manuel Terrés Haro graduated in Electronics Engineering and Automation in 2016, he received his M.Sc. degree in Biomedical Engineering in 2018, both titles by Universitat Politécnica de Valéncia (UPV). He is a Ph.D. student in the (UPV) Electronics department. His main research area is the development of laboratory equipment for experimental applications, electronic design, firmware and software programming and simulation modelization.

Andy Hernández Montoto graduated in Chemistry at the University of Havana (UH) in 2011. He received his M.Sc.degree in Chemistry at (UH) in 2014. He received his Ph.D. in 2019 at Universitat Politécnica de Valéncia (UPV) and his main research area is the development of nanodevice based on gold nanoparticles and mesoporous silica nanoparticles for drug photorelease applications using near infrared radiations.

Maria Pardo Huguet graduated in Electronics Engineering and Automation in 2018, she received her M.Sc. degree in Biomedical Engineering in 2020, both titles by Universitat Politécnica de Valéncia (UPV). She is currently teaching in a secondary school.

Cristina de la Torre graduated in Chemistry at the Universitat de Valéncia in 2010, and received her M.Sc. degree from the same university in 2011. She received her Ph.D. and is currently teaching in a secondary school. Her main area of interest is the development of gated materials for advanced applications.

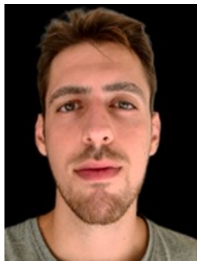

Javier Monreal Trigo has M.Sc. degrees from Universitat Politécnica de Valéncia (UPV) both in Electronic Engineering (Power Electronics) (2018) and Data Analysis (2019). He is pursuing Ph.D. through the University Professor Training (FPU) fellowship. His main areas of interest are digital and analog electronic design (PCB, VLSI, HDL), including GUI, microcontroller programming and communications; as well as data analysis, multivariate models and artificial intelligence. Nowadays is researching in the fields of electrically controlled drug release, nervous tissue electrostimulation, ultra-selective biochemical sensors, electronic tongues and optochemogenetics.

Javier Ibañez has a M.Sc. in Power Electronic and Control from the Université Pierre et Marie Curie (Paris VI), awarded in 1994. He received his Ph.D. in 2009 at the Universidad Politécnica de Valencia (UPV). He is an assistant professor of Electronic Technology in the Electronic Engineering Department of the UPV. He is a member of the Interuniversity Research Institute for Molecular Recognition and Technological Development. His main areas of interest are optical devices for water and air contamination detection.

Rafael Masot has MSc degrees from Universitat de Valéncia, Spain, both in Physics (1991) and Electronic Engineering (1996). He completed his doctorate in 2010 at the Universidad Politécnica de Valencia (UPV). He is Lecturer at the Electronic Engineering Department of the UPV, currently teaching in the B.Sc. Degrees in Aerospace Engineering and Industrial Electronics and Automation Engineering; and also in the M.Sc. Degree in Sensors for Industrial Applications. He is a member of Interuniversity Research Institute for Molecular Recognition and Technological Development. His main areas of research interest are physical sensors and instrumentation.

Ramón Martínez Máñez graduated in chemistry from the University of Valencia in 1986, received his Ph.D. in 1990 from the same university. After a postdoctoral period at Cambridge (UK), he joined the Department of Chemistry at the Universidad Politécnica deValencia. He became a full professor in 2002. His main areas of interest are in the field of chromofluorogenic and electrochemical sensors and molecular probes for anions, cations and neutral chemical species. He is also interested in the design of smart controlled delivery systems.

Eduardo García Breijo obtained his M.Sc. degree in Electronic Engineering from the Universidad Politécnica de Valencia (UPV) in 1997, and received his Ph.D. in 2004, also from the UPV. He is an Assistant Professor of the Electronics Engineering Department of the UPV. He is a member of the Interuniversity Research Institute for Molecular Recognition and Technological Development. His main areas of interest are the development of multisensors in thick-film technology, design of electronic systems and neural networks.